Coaxial-structured ZnO/silicon nanowires extended-gate field-effect transistor as pH sensor

Hung-Hsien Li [a,*], Chi-En Yang [b], Chi-Chung Kei [c], Chung-Yi Su [d], Wei-Syuan Dai [a], Jung-Kuei Tseng [b], Po-Yu Yang [a], Jung-Chuan Chou [e], Huang-Chung Cheng [a]

[a] Department of Electronics Engineering and Institute of Electronics, National Chiao Tung University, Hsinchu 30010, Taiwan
[b] Department of Electronics Engineering, St. John's University, Taipei 25135, Taiwan
[c] Instrument Technology Research Center, National Applied Research Laboratories, Hsinchu 30076, Taiwan
[d] Department of Materials Science and Engineering, National Tsing Hua University, Hsinchu 30013, Taiwan
[e] Graduate School of Electronic Engineering, National Yunlin University of Science and Technology, Yunlin 64002, Taiwan

ARTICLE INFO

ABSTRACT

An extended-gate field-effect transistor (EGFET) of coaxial-structured ZnO/silicon nanowires as pH sensor was demonstrated in this paper. The oriented 1-μm-long silicon nanowires with the diameter of about 50 nm were vertically synthesized by the electroless metal deposition method at room temperature and were sequentially capped with the ZnO films using atomic layer deposition at 50 °C. The transfer characteristics (I_{DS}–V_{REF}) of such ZnO/silicon nanowire EGFET sensor exhibited the sensitivity and linearity of 46.25 mV/pH and 0.9902, respectively for the different pH solutions (pH 1–pH 13). In contrast to the ZnO thin-film ones, the ZnO/silicon nanowire EGFET sensor achieved much better sensitivity and superior linearity. It was attributed to a high surface-to-volume ratio of the nanowire structures, reflecting a larger effective sensing area. The output voltage and time characteristics were also measured to indicate good reliability and durability for the ZnO/silicon nanowires sensor. Furthermore, the hysteresis was 9.74 mV after the solution was changed as pH 7 → pH 3 → pH 7 → pH 11 → pH 7.

1. Introduction

pH determination was necessary for many biochemical and biological processes. In 1970, Bergveld proposed the ion-sensitive field-effect transistor (ISFET) in neurophysiological measurement [1]. Recently, there were many studies introducing extended-gate field-effect transistor (EGFET) as an alternative for the fabrication of ISFET [2,3]. EGFET exhibited many advantages over the conventional ISFET, such as low cost, simpler packaging, temperature and light insensitivity, flexibility of shape of the extended-gate structure, and better long-term stability [4–7].

Moreover, there were many investigations focused on the sensing membranes of EGFET such as zinc oxide (ZnO) [8], tin oxide (SnO$_2$) [9], ruthenium oxide (RuO$_2$) [10], and vanadium oxide (V$_2$O$_5$) [11], etc. ZnO, with a direct band gap of $Eg = 3.37$ eV and a high exciton binding energy of 60 meV at room temperature, was a promising material for the biosensor application because of their nontoxicity, biosafety, biocompatibility, and high electron communication features [12].

Based on the site-binding model, the chemical sensitivity was depended on the total number of surface sites per unit area (N_S). Many researches suggested that the larger N_S had the better pH sensitivity and superior linearity [13,14]. Consequently, one-dimensional nanostructures such as nanorods, nanowires, and nanotubes had attracted a lot of attention for the pH sensing due to their high surface-to-volume ratio.

In this paper, a simple and low temperature method was proposed to fabricate such a coaxial-structured nanowire sensor, based on the electroless metal deposition (EMD) and atomic layer deposition (ALD) methods. As compared with ZnO nanowires, ZnO/silicon nanowire structures could be easily controlled for nanowire diameter, length and spacing through the different etching conductions such as etching times, and solution concentrations. The dense well-aligned silicon nanowires (SiNWs) provided higher surface areas for H$^+$ sensing. Our result demonstrated superior sensitivity and better linearity than the ZnO nanowire sensor [15]. It revealed the potential applications in pH sensing using ZnO/silicon nanowires.

2. Experiment details

The well-aligned SiNWs were synthesized by EMD method at room temperature. At first, the p-type (100) silicon substrates were cleaned

---

* Corresponding author. Tel./fax: +886 3 5738343.
E-mail address: et248854.ee97g@nctu.edu.tw (H.-H. Li).

with sulfuric acid (H_2SO_4:$H_2O_2 = 3$:1), rinsed with deionized water, and then soaked in dilute Hydrofluoric acid (HF:$H_2O = 1$:100). Next, the cleaned silicon substrates were immersed in mixed $AgNO_3$ and HF aqueous etching solutions at room temperature. The concentrations of $AgNO_3$ and HF were 0.02 M and 5 M, respectively. Subsequently, the silicon substrates were immersed in nitric acid (70%) to remove the masking Ag particles. Finally, the silicon substrates were rinsed in deionized water and then dried. The wire length of SiNWs could be effectively controlled by adjusting the etching time. In this study, the etching time was controlled as 3 min and the 1-μm-long SiNWs with the diameter of about 50 nm were obtained. After the SiNWs were formed, they were sequentially capped with the ZnO films by ALD using $Zn(C_2H_5)_2$ (DEZ) and H_2O as the precursors at 50 °C. Each cycle consisted of a precursor pulse and a N_2 purge. The pulse time and the purge time for both DEZ precursor and H_2O precursor were 0.3 s and 5 s, accordingly. The deposition pressure was controlled as 133.322 Pa and the growth rate of ZnO films was about 1.2 Å/cycle.

Furthermore, the silver paste served as the electrode was applied to the silicon substrate. The metal wire was bound with silver paste and packaged with epoxy resin. Subsequently, the packaged electrode was dried in an oven at 120 °C for 30 min. Epoxy resin was used to define the sensing window at 2×2 mm^2. The sensing membrane and the reference electrode (Ag/AgCl) were immersed in the different pH solutions and connected to the commercial standard metal–oxide–semiconductor field-effect transistor (MOSFET) device (CD4007UB). The drift effect and hysteresis measurement consisted of a commercial instrumentation amplifier (IC LT1167) and digital multi-meter (HP 34401A). All measurements were carried out in a dark box at room temperature in order to avoid the light and temperature interferences.

Surface morphologies of the ZnO/silicon nanowires were observed by field-emission scanning electron microscopy (FE-SEM, Hitachi S-4700I). The operating voltage and current were set at 15 keV and 10 μA. The crystalline structure of the ZnO/silicon nanowires was investigated using high resolution X-ray diffractometer (Bede D1). The radiation source is Cu Kα ($\lambda = 1.5405$ Å) operated at 40 kV and 40 mA. The measurement was performed in the θ–2θ configuration with a 0.1° step size and a 1 s count per step.

3. Results and discussion

Fig. 1(a) shows the 45° tilted and cross-sectional (inset) FE-SEM images of the as-synthesized SiNWs using EMD method. The dense well-aligned SiNWs were observed over the entire substrate. The diameter and wire length of the SiNWs could be effectively controlled by adjusting the etching time. The etching time is controlled as 3 min. The average diameter and wire length of the SiNWs are around 50 nm and 1 μm, correspondingly. After the SiNWs were capped with ZnO films by ALD, the SiNWs became larger and circular, as shown in Fig. 1(b). It was found that the individual SiNWs were conformally covered with the ZnO films. Approximately 50 nm-thick ZnO films were deposited on the SiNWs by applying 400 cycles of ALD.

The glancing-angle X-ray diffraction of the ZnO/silicon nanowires is shown in Fig. 2. The spectrum reveals that the deposited films are the hexagonal wurzite ZnO with lattice constants of $a = 3.24$ Å and $c = 5.19$ Å. It indicates that the ZnO films deposited at 50 °C in ALD is polycrystalline. Furthermore, the broadened X-ray diffraction peaks suggest the smaller grain size of the ZnO films. It implies that there are more oxygen vacancies existing in the ZnO films.

Fig. 3 shows the Raman spectrum of the ZnO/silicon nanowires under a 488 nm laser illumination. The Raman peak at 520 cm^{-1} is attributed to crystalline silicon. The Raman at 437 and 581 cm^{-1} indicated in the Fig. 3 (inset) are attributed to the E_2 high frequency mode, namely E_2(high), and the A_1 longitudinal optical phonon mode, namely A_1(LO), of ZnO. The optical phonons mode of A_1 is the Raman and infrared actives, whereas the E_2 mode is the Raman active only [16].
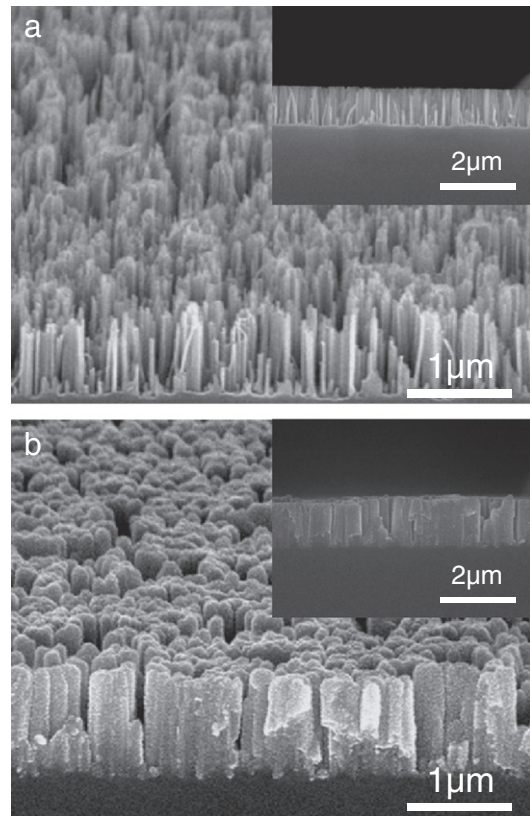

Fig. 1. (a) 45° tilted and cross-sectional (inset) FE-SEM images of the as-synthesized SiNWs. (b) 45° tilted and cross-sectional (inset) FE-SEM images of the SiNWs capped with ZnO films.

The relation between the drain-source current (I_{DS}) and pH value can be obtained using the basic MOSFET expression [17]. For the linear region

$$I_{DS} = \frac{W\mu_n C_{OX}}{2L}\left[2(V_{GS} - V_T)V_{DS} - V_{DS}^2\right]$$

and for the saturation region

$$I_{DS} = \frac{W\mu_n C_{OX}}{2L}\left[(V_{GS} - V_T)^2\right]$$

where W/L is the channel width-to-length ratio, μ_n is the electron mobility in the channel, C_{OX} is the gate capacitance per unit area, V_{GS} is
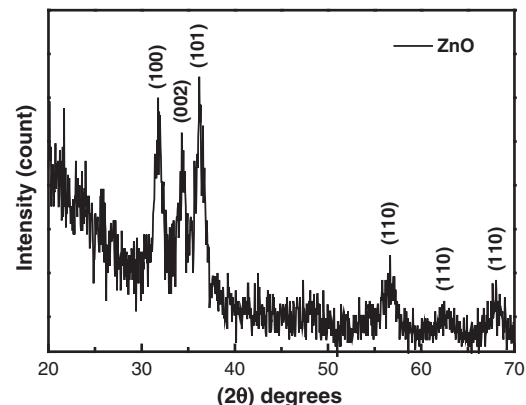

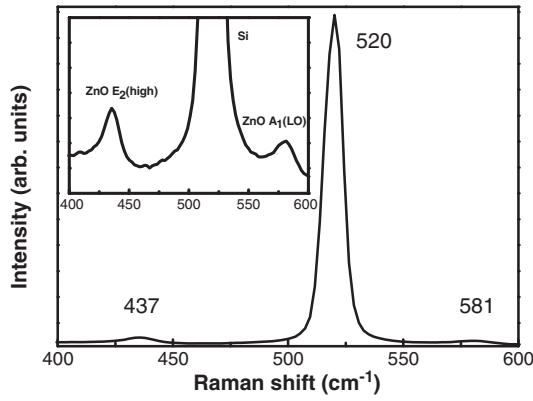**Fig. 2.** Glancing-angle X-ray diffraction of the ZnO/silicon nanowires.

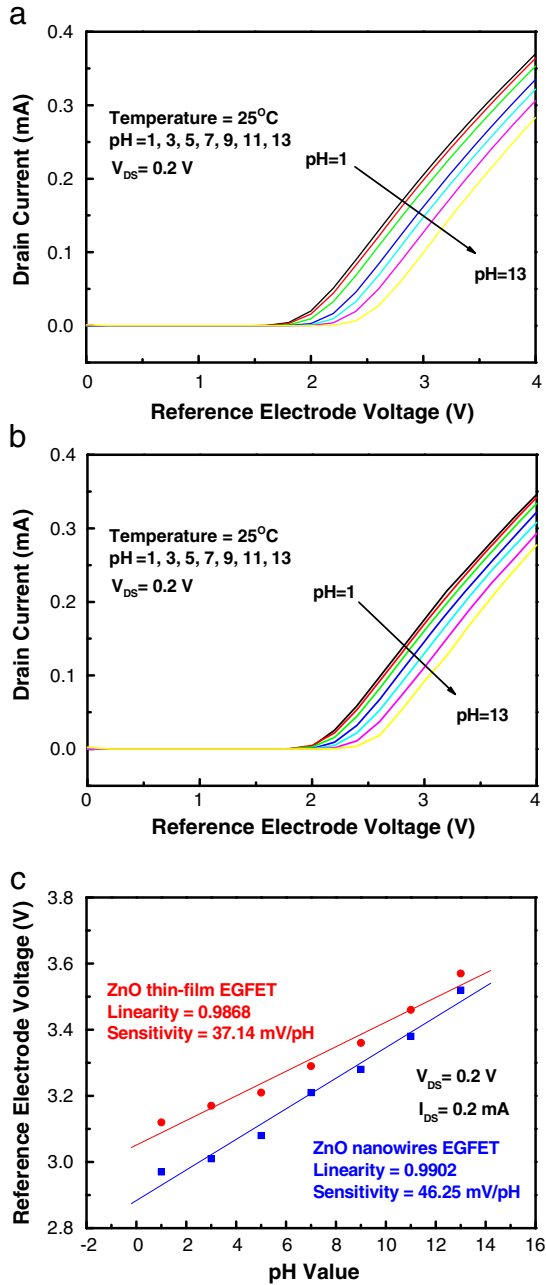Fig. 3. Raman spectrum of the ZnO/silicon nanowires.

the reference electrode voltage (V_{REF}), V_{DS} is the drain-source voltages, and V_T is the threshold voltage of EGFET sensor and related to pH value.

The transfer characteristics (I_{DS}–V_{REF}) of the ZnO/silicon nanowire EGFET sensor in the linear region (for V_{DS} fixed at 0.2 V, while V_{REF} scanned from 0 to 4 V) from pH 1 to pH 13 are shown in Fig. 4(a). It is observed that the threshold voltage shift depends upon the pH value, i.e., the threshold voltage shifts from the left to the right with increasing pH value. Fig. 4(b) displays I_{DS}–V_{REF} measurements of the ZnO/silicon thin-film one in the linear region. Fig. 4(c) exhibits the sensitivity and linearity of the ZnO/silicon nanowires and thin-film EGFET sensors. The result indicates that V_{REF} depends linearly on pH value in the linear region (for I_{DS} fixed at 0.2 mA). The sensitivity and linearity of the ZnO/silicon nanowire EGFET sensor are 46.25 mV/pH and 0.9902, respectively. Moreover, the sensitivity and linearity of the ZnO thin-film one are 37.14 mV/pH and 0.9868, accordingly.
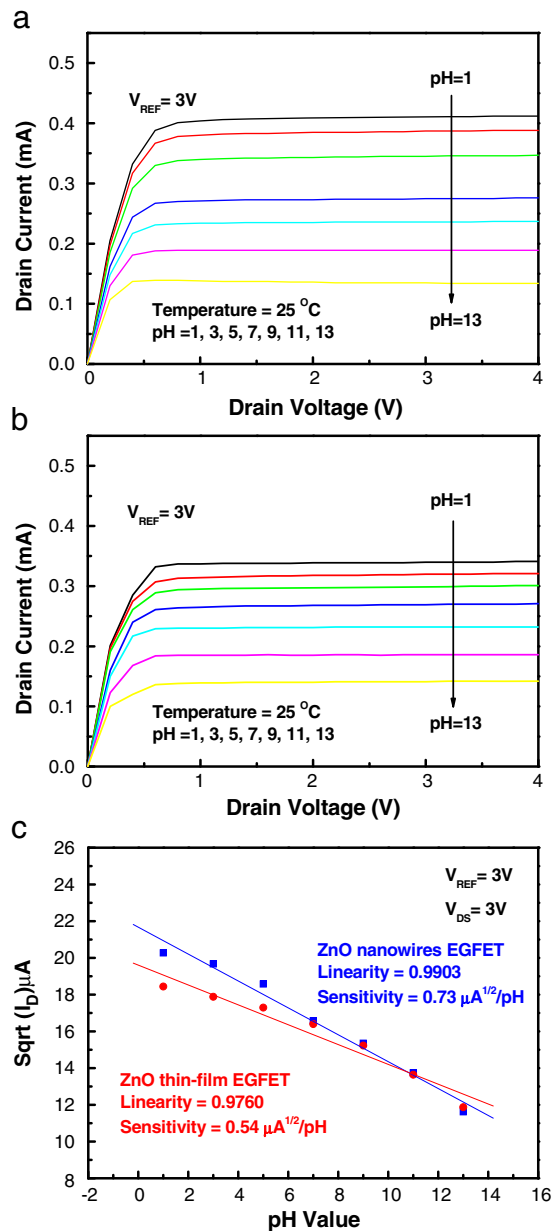

Fig. 4. (a) and (b) I_{DS}–V_{REF} measurements of the ZnO/silicon nanowires and thin-film EGFET sensors. (c) Sensitivity and linearity of the ZnO/silicon nanowires and thin-film EGFET sensors in the linear region.

Fig. 5. (a) and (b) I_{DS}–V_{DS} measurements of the ZnO/silicon nanowires and thin-film EGFET sensors. (c) Sensitivity and linearity of the ZnO/silicon nanowires and thin-film EGFET sensors in the saturation region.
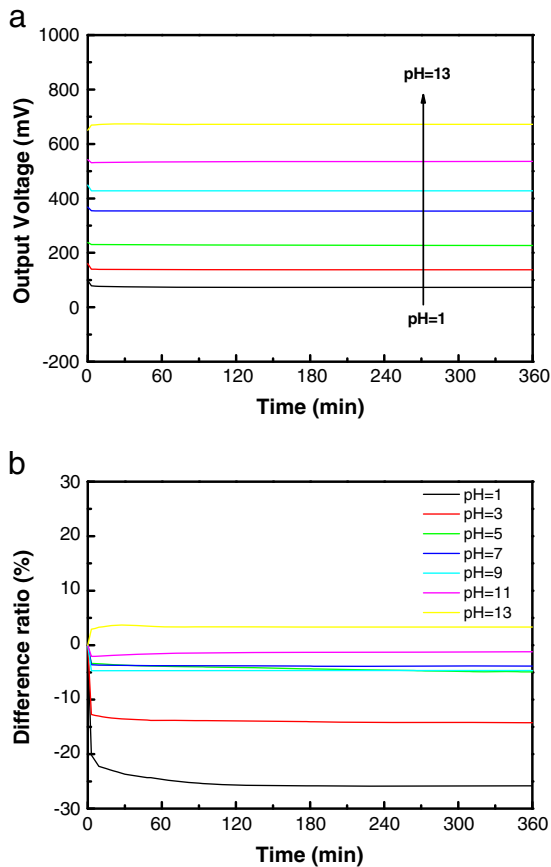
Fig. 6. (a) V–t measurements and (b) difference ratios of the ZnO/silicon nanowire EGFET sensor.

Fig. 7. Hysteresis characteristics of the ZnO/silicon nanowire EGFET sensor.

The output characteristics (I_{DS}–V_{DS}) of the ZnO/silicon nanowires EGFET sensor in the saturation region (for V_{REF} fixed at 3 V, while V_{DS} scanned from 0 to 4 V) from pH 1 to pH 13 are shown in Fig. 5(a). It is observed that the drain current decreases with increasing pH value, i.e., the drain current shifts from the bottom to the top with increasing pH value. Fig. 5(b) displays I_{DS}–V_{DS} measurements of the ZnO/silicon thin-film one in the saturation region. Fig. 5(c) exhibits the sensitivity and linearity of the ZnO/silicon nanowires and thin-film EGFET sensors. The result indicates that $\sqrt{I_{DS}}$ depends linearly on pH value in the saturation region (for V_{DS} fixed at 3 V). The sensitivity and linearity of the ZnO/silicon nanowire EGFET sensor are 0.73 mA$^{1/2}$/pH and 0.9903, respectively. Moreover, the sensitivity and linearity of the ZnO thin-film one are 0.54 mA$^{1/2}$/pH and 0.9760, accordingly.

Consequently, the ZnO/silicon nanowire EGFET sensor demonstrates the better sensitivity and superior linearity as compared with the ZnO one. It is attributed to a high surface-to-volume ratio of the nanowire structure and can provide more surface sites and larger effective sensing areas. Moreover, the polycrystalline ZnO films deposited by ALD implied that the more oxygen vacancies could effectively sense with H$^+$ concentration.

The drift effect has been used to evaluate reliability and durability of electrochemical sensors. Fig. 6(a) reveals the output voltage and time (V–t) measurements of the ZnO/silicon nanowires EGFET for a duration (i.e., 0–360 min) with different pH solutions. The output voltage increases with increasing pH value. The difference ratios have also been calculated in Fig. 6(b). It shows that the difference ratios of the device are less than 5% in pH = 5–13, 25% in pH = 1 and
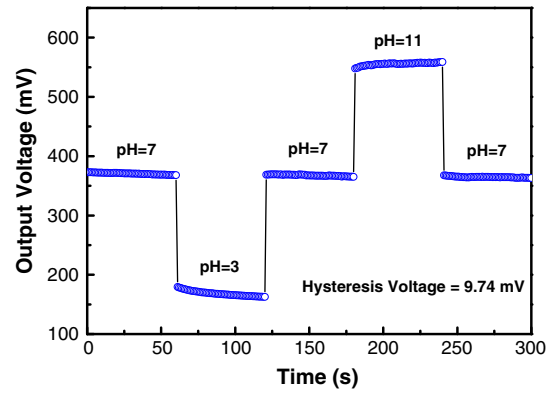
15% in pH = 3. It demonstrates the good reliability and durability of the ZnO/silicon nanowire EGFET sensor for 360 min durations.

Fig. 7 displays the hysteresis characteristics of the ZnO/silicon nanowire EGFET sensor. The output offset voltage is measured at 1 minute intervals between solutions with different pH values. The result indicates that the hysteresis is 9.74 mV after the solution is changed as pH 7 → pH 3 → pH 7 → pH 11 → pH 7.

4. Conclusion

Coaxial-structured ZnO/silicon nanowire EGFET as pH sensor has been proposed to achieve the higher sensitivity of 46.25 mV/pH and larger linearity of 0.9902 in the linear region. Furthermore, it also showed a better sensitivity of 0.73 mA$^{1/2}$/pH and a greater linearity of 0.9903 in the saturation region. It was attributed to a high surface-to-volume ratio of the nanowire structure, reflecting a larger effective sensing area and more oxygen vacancies. The V–t measurements and the hysteresis characteristics of ZnO/silicon nanowires EGFET also indicated the good reliability and durability. There such low-temperature-fabricated ZnO/silicon nanowires revealed the potential for flexible and disposable biosensors.

References

[1] P. Bergveld, IEEE Trans. Biomed. Eng. 17 (1970) 70.
[2] J.V.D. Spiegel, I. Lauks, P. Chan, D. Babic, Sens. Actuators B 4 (1983) 291.
[3] T. Katsube, M. Katoh, H. Maekawa, M. Hara, Sens. Actuators B 1 (1990) 504.
[4] L.L. Chi, L.T. Yin, J.C. Chou, W.Y. Chung, T.P. Sun, K.P. Hsiung, S.K. Hsiung, Sens. Actuators B 71 (2000) 68.
[5] J.C. Chou, J.L. Chiang, C.L. Wu, Jpn. J. Appl. Phys. Part 1 44 (2005) 4838.
[6] J.L. Chiang, J.C. Chou, Y.C. Chen, J. Med. Biol. Eng. 21 (2001) 135.
[7] N.H. Chou, J.C. Chou, T.P. Sun, S.K. Hsiung, Sens. Actuators B 130 (2008) 359.
[8] P.D. Batista, M. Mulato, Appl. Phys. Lett. 87 (2005) 143508.
[9] P.D. Batista, M. Mulato, C.F.O. Graeff, F.J.R. Fernandez, F.D. Marques, Braz. J. Phys. 36 (2006) 478.
[10] J.C. Chou, D.J. Tzeng, Rare Met. Mater. Eng. 35 (2006) 256.
[11] E.M. Guerra, G.R. Silva, M. Mulato, Solid State Sci. 11 (2009) 456.
[12] S.M. Al-Hilli, M. Willander, A. Öst, P. Strålfors, J. Appl. Phys. 102 (2007) 084304.
[13] H.K. Liao, J.C. Chou, W.Y. Chung, T.P. Sun, S.K. Hsiung, Mater. Chem. Phys. 59 (1999) 6.
[14] J.L. Chiang, Y.C. Chen, J.C. Chou, Jpn. J. Appl. Phys. 40 (2001) 5900.
[15] A. Fulati, S.M. Usman Ali, M. Riaz, G. Amin, O. Nur, M. Willander, Sensors 9 (2009) 8911.
[16] R. Cuscó, E.A. Lladó, J. Ibáñez, L. Artús, Phys. Rev. B 75 (2007) 165202.
[17] S.M. Sze, Physics of Semiconductor Devices, 2nd ed. Wiley, New York, 1981.